

Rapid #: -20934669

CROSS REF ID: **10965922920005671**

LENDER: **JMS (Hebrew University: Humanities and Social Sciences) ::
Main Library**

BORROWER: **LT1 (University of Technology Sydney) :: Blake Library**

TYPE: Article CC:CCG

JOURNAL TITLE: Physics in medicine and biology

USER JOURNAL TITLE: Physics in medicine & biology.

ARTICLE TITLE: Optimising multi-target multileaf collimator tracking using real-time dose for locally advanced prostate cancer patients

ARTICLE AUTHOR: Hewson, Emily A ; Nguyen, Doan Trang ; Le, Andrew

VOLUME: 67

ISSUE: 18

MONTH:

YEAR: 2022-09-21

PAGES: 185003

ISSN: 0031-9155

OCLC #: 34482128

Processed by RapidX: 6/26/2023 2:00:55 AM

This material may be protected by copyright law (Title 17 U.S. Code)

PAPER

Optimising multi-target multileaf collimator tracking using real-time dose for locally advanced prostate cancer patients

To cite this article: Emily A Hewson *et al* 2022 *Phys. Med. Biol.* **67** 185003

View the [article online](#) for updates and enhancements.

You may also like

- [Multileaf collimator tracking integrated with a novel x-ray imaging system and external surrogate monitoring](#)
Andreas Krauss, Martin F Fast, Simeon Nill *et al.*
- [Geometric uncertainty analysis of MLC tracking for lung SABR](#)
Vincent Caillet, Benjamin Zwan, Adam Briggs *et al.*
- [Real-time intrafraction motion monitoring in external beam radiotherapy](#)
Jenny Bertholet, Antje Knopf, Björn Eiben *et al.*

SunCHECK[®]

Powering Quality Management in Radiation Therapy

See why 1,600+ users have chosen SunCHECK for automated, integrated Patient QA and Machine QA.

[Learn more >](#)



**Demo
SunCHECK
at ESTRO:
Booth # 150**



SUN NUCLEAR



PAPER

Optimising multi-target multileaf collimator tracking using real-time dose for locally advanced prostate cancer patients

Emily A Hewson¹ , Doan Trang Nguyen^{1,2,3} , Andrew Le³, Jeremy T Booth^{3,4}, Paul J Keall¹ and Lars Mejnertsen¹ ¹ ACRF Image X Institute, University of Sydney Medical School, Sydney, Australia² School of Biomedical Engineering, University of Technology Sydney, NSW, Australia³ Northern Sydney Cancer Centre, Royal North Shore Hospital, Sydney, Australia⁴ School of Physics, University of Sydney, Sydney, AustraliaE-mail: emily.hewson@sydney.edu.au**Keywords:** MLC tracking, multi-target tracking, real-time adaptive radiotherapy, motion managementRECEIVED
11 April 2022REVISED
3 August 2022ACCEPTED FOR PUBLICATION
12 August 2022PUBLISHED
13 September 2022**Abstract**

Objective. The accuracy of radiotherapy for patients with locally advanced cancer is compromised by independent motion of multiple targets. To date, MLC tracking approaches have used 2D geometric optimisation where the MLC aperture shape is simply translated to correspond to the target's motion, which results in sub-optimal delivered dose. To address this limitation, a dose-optimised multi-target MLC tracking method was developed and evaluated through simulated locally advanced prostate cancer treatments. *Approach.* A dose-optimised multi-target tracking algorithm that adapts the MLC aperture to minimise 3D dosimetric error was developed for moving prostate and static lymph node targets. A fast dose calculation algorithm accumulated the planned dose to the prostate and lymph node volumes during treatment in real time, and the MLC apertures were recalculated to minimise the difference between the delivered and planned dose with the included motion. Dose-optimised tracking was evaluated by simulating five locally advanced prostate plans and three prostate motion traces with a relative interfraction displacement. The same simulations were performed using geometric-optimised tracking and no tracking. The dose-optimised, geometric-optimised, and no tracking results were compared with the planned doses using a 2%/2 mm γ criterion. *Main results.* The mean dosimetric error was lowest for dose-optimised MLC tracking, with γ -failure rates of 12% \pm 8.5% for the prostate and 2.2% \pm 3.2% for the nodes. The γ -failure rates for geometric-optimised MLC tracking were 23% \pm 12% for the prostate and 3.6% \pm 2.5% for the nodes. When no tracking was used, the γ -failure rates were 37% \pm 28% for the prostate and 24% \pm 3.2% for the nodes. *Significance.* This study developed a dose-optimised multi-target MLC tracking method that minimises the difference between the planned and delivered doses in the presence of interfraction motion. When applied to locally advanced prostate cancer, dose-optimised tracking showed smaller errors than geometric-optimised tracking and no tracking for both the prostate and nodes.

Introduction

Radiotherapy for patients with locally advanced cancer can require multiple targets to be irradiated simultaneously, however differential motion of these targets (Pantarotto *et al* 2009, Weiss *et al* 2012, Schmidt *et al* 2016, Kershaw *et al* 2018) can result in decreased treatment accuracy (Hwang *et al* 2012, van Elmpt *et al* 2012). Currently available adaptation systems, such as the CyberKnife (Kilby *et al* 2010) or Radixact (Schnarr *et al* 2018) involve specialised treatment systems that adapt the radiation to a target's motion in real time. However, currently available commercial systems are not able to adapt to multiple targets that have independent motion. Multileaf collimator (MLC) tracking (Sawant *et al* 2008, Falk *et al* 2010, Keall *et al* 2021) can be implemented on standard clinical systems and has been utilised to develop a multi-target tracking method that

was demonstrated to track multiple independent targets in a simulation study (Hewson *et al* 2021a), as well as experimentally on a standard linac (Hewson *et al* 2021b) and an MRI-linac (Liu *et al* 2020).

Previous implementations of MLC tracking were performed using a geometric optimisation approach. Geometric-optimised tracking adapts the MLC leaf positions such that the 2D fluence of the radiation beam passing through a moving target and surrounding tissue is consistent with what was planned (Sawant *et al* 2008), minimising the 2D overexposure and underexposure to the tissue at that timestep (Ruan and Keall 2011, Moore *et al* 2016). However, the exposure of the target seen in 2D from the beam's-eye-view (BEV) is not representative of the 3D dose that has been delivered to the tissue, which is more closely linked to clinical patient outcomes from radiotherapy (Dale 1996, Olsson *et al* 2018, Grimm *et al* 2021). Thus, it would be advantageous to adapt the treatment based on the 3D dose over 2D geometry.

While clinical applications of geometric-optimised MLC tracking have been demonstrated to deliver a dose distribution closer to the plan than what would be delivered using the standard of care (Keall *et al* 2018a, 2018b, Booth *et al* 2021), limitations with the MLC tracking method, including the limited leaf width and speeds, can result in dosimetric error (Poulsen *et al* 2012a). Geometric-optimised MLC tracking does not account for the errors that accumulate throughout a treatment, instead only optimising for the 2D geometry at each timestep throughout the treatment. In addition to these limitations, multi-target MLC tracking was also found to result in dosimetric error due to limitations with forming an adapted aperture for independently moving targets that overlap in the BEV (Hewson *et al* 2021a, 2021b).

To address the limitations of the previous MLC tracking algorithm, a novel MLC tracking method that optimises the adapted leaf positions to the 3D dose in real-time was developed by Mejnertsen *et al* (2021). This dose-optimised MLC tracking method incorporates a real-time 3D dose accumulation method to calculate the MLC leaf positions that correct for motion, as well as the dosimetric errors that occur throughout a treatment. Dose-optimised MLC tracking was found to reduce the delivered dosimetric error compared to geometric-optimised tracking for single-target prostate tracking with a mean computation time within 40 ms for each aperture.

The aim of the current study was to further develop dose-optimised MLC tracking for the implementation of multi-target tracking. The performance of dose-optimised multi-target MLC tracking was evaluated through simulated treatments for locally advanced prostate cancer patients and was compared to the previously used geometric-optimised multi-target MLC tracking algorithm, and standard of care treatment with no tracking.

Methods

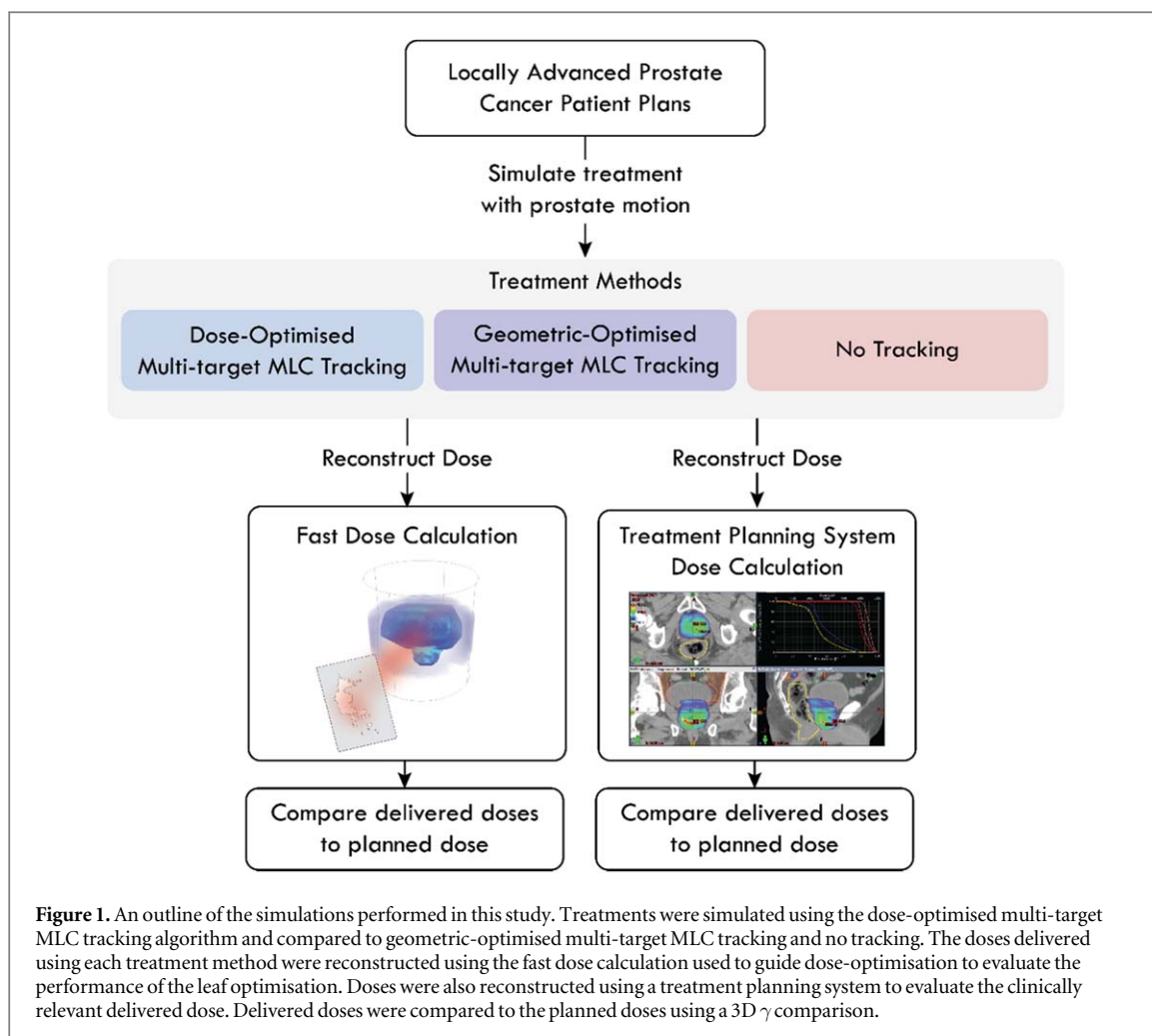
An outline of the study is summarised in figure 1.

Dose-optimised multi-target MLC tracking

A multi-target MLC tracking method that adapts to independently moving targets by re-optimising the MLC leaf positions based on the delivered dose was developed. The steps performed for multi-target dose-optimised MLC tracking method are described below and summarised in figure 2.

Prior to treatment, a 3D volume was generated containing dose points arranged in a staggered grid with a spacing of 2 mm along each 3D axis. The dose delivered during treatment was accumulated on these points, referred to as the dose point cloud. A unique dose point cloud was generated for each patient, where the prostate and lymph node point clouds were created based on the respective planning target volume (PTV) contours, and each point cloud was expanded by 1 cm in each direction to encompass the dose fall-off outside of the target and to ensure that there are no gaps in dose points within the MLC apertures. The convex hull of the lymph node PTV was then generated as a boundary for the point cloud so that dose points could be arranged within this boundary to fill the empty space in the centre the lymph nodes. The prostate point cloud was not expanded in the superior direction and the lymph node point cloud was not expanded in the inferior direction as this was the region where the targets overlapped. Each dose point was labelled as either belonging to the prostate or lymph nodes. As the prostate PTV and lymph node PTVs overlap, separate dose points are generated for each target and can exist within the same region of space but undergo independent motion during treatment simulation.

A detailed description of the dose optimisation algorithm, including equations used, can be found in Mejnertsen *et al* (2021). A brief description of the algorithm is included below. During the treatment, the dose optimisation process occurs over several iterations. At each timestep, the planned dose that is delivered to the dose point cloud up until that timepoint was calculated based on the planned MLC apertures. The 3D dose calculation method was performed by accounting for the gantry angle, collimator angle, and MLC leaf positions, and used a simple line-of-sight dose calculation, where one dose unit is deposited to all dose points that are



exposed within the open aperture. To ensure fast dose calculation factors such as beam divergence, attenuation and heterogeneous tissue composition were not considered.

Once the planned dose for that iteration was calculated, the dose points assigned to the prostate are shifted independently to correspond to the prostate's displacement at that point in the treatment. The dose points that are assigned to the lymph nodes remain stationary. This planned dose with the shifted dose points indicates the desired dose to be delivered considering the plan and target motion.

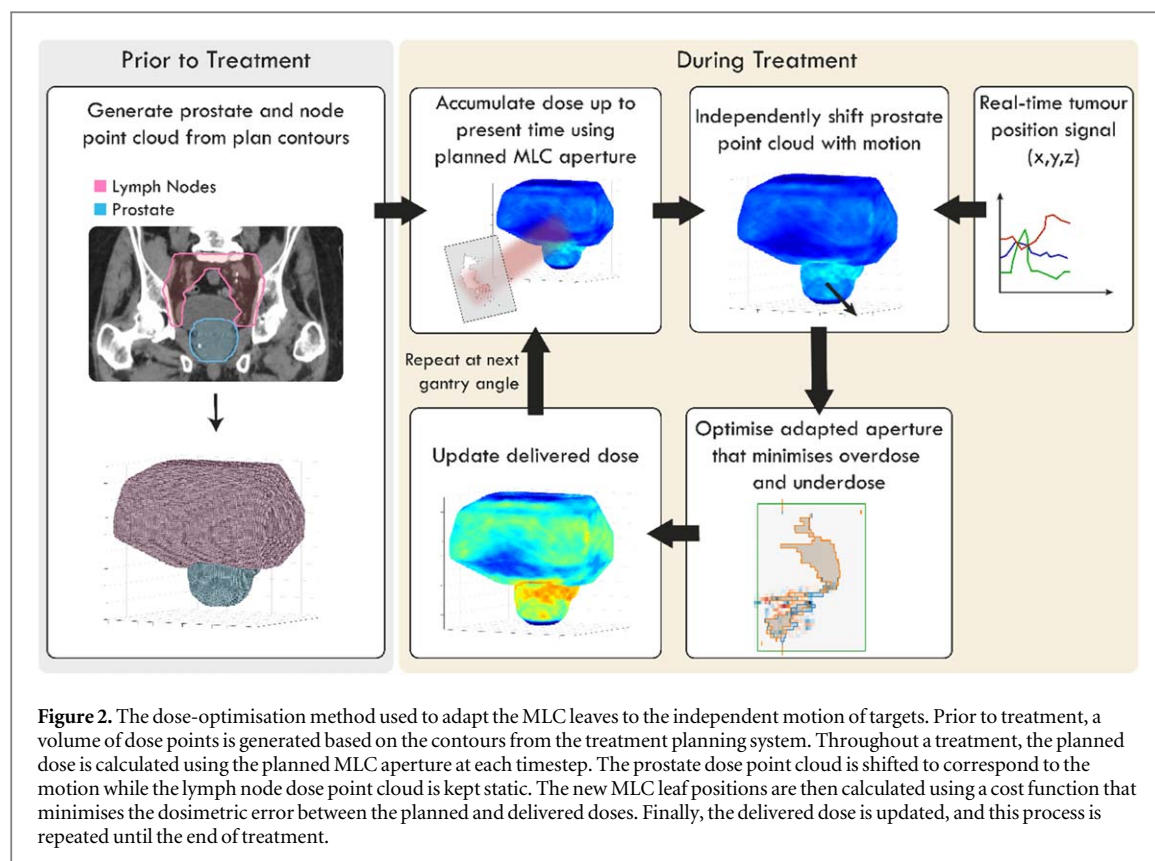
This 3D shifted planned dose was then projected onto the 2D BEV plane by integrating all dose points along the gantry axis. The difference between the shifted planned dose and the dose that has been delivered up until the timepoint was used to optimise the MLC positions. For each leaf pair, the dose cost was calculated and the leaf positions that minimise that cost were selected for the adapted aperture.

Once the adapted leaf positions have been calculated and adjusted, the delivered dose to the dose point cloud was updated, and this process repeated for each timestep until the end of treatment. The mean computation time for dose accumulation at each timestep was 32 ± 10 ms, and each aperture optimisation took 47 ± 13 ms.

Treatment simulations

To evaluate the performance of dose-optimised multi-target MLC tracking, the algorithm was tested *in silico* and compared to the geometric-optimised multi-target MLC tracking method which has been described in further detail by Hewson *et al* (2021a), as well as standard of care treatment where motion for each target is not managed during treatment.

Each treatment method was evaluated by simulating treatment where the prostate undergoes relative motion to the pelvic lymph nodes. Five treatment plans for patients with locally advanced prostate cancer were selected, which had prescription doses of 60 Gy delivered over 20 fractions, delivered using volumetric modulated arc therapy (VMAT). The plans were each generated with three 358° arcs with gantry rotation covering 181° – 179° . While standard treatments for locally advanced cancer patients previously planned the collimator angles to 10° , 350° , and 0° , the plans in this study were generated with collimator angles of 45° , 315° ,



and 45° as these angles are favourable for the performance of dose-optimised MLC tracking. The jaws were also expanded by 1 cm in each direction to allow for motion to be tracked.

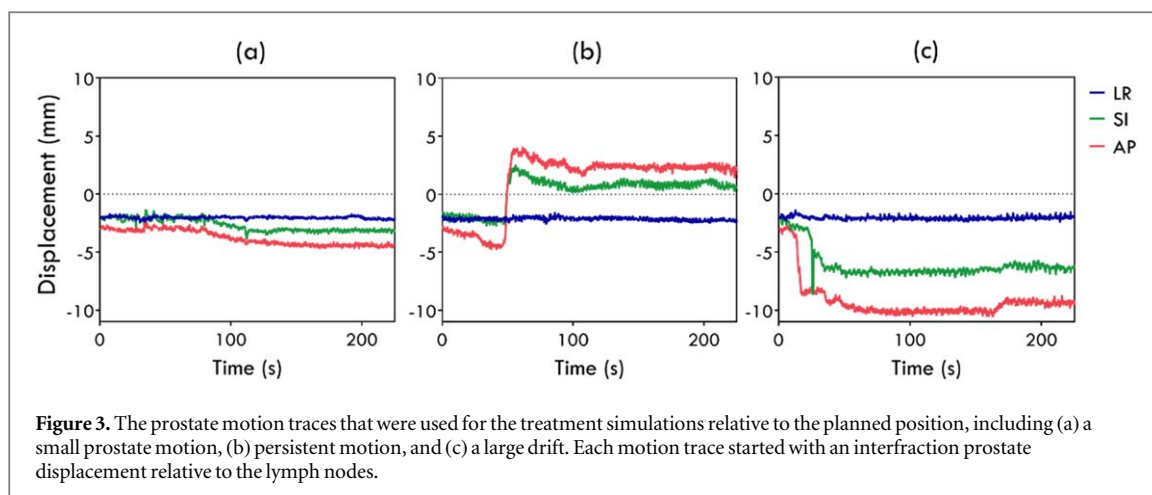
The physical leaf limitations including leaf widths and velocity were based on a Millennium 120-leaf MLC for the treatment simulations performed in this study. To simulate deliverable MLC apertures, the limited leaf velocity was taken into account during the leaf-optimisation step such that the maximum distance that could be travelled at each timestep was limited by a speed of 3.6 cm s^{-1} (Wijesooriya *et al* 2005). Gantry trajectory was based on treatment log files from patient treatment.

Three intrafraction prostate motion traces measured during patient treatment by Langen *et al* (2008) were selected to represent a range of motion that the prostate could undergo. Treatments were simulated using these three prostate motions for each of the five locally advanced prostate patients. For locally advanced prostate cancer treatments, the displacement of the prostate relative to the lymph nodes may be different at the beginning of treatment compared to the planning computed tomography (CT) image. To simulate this scenario, an interfraction prostate displacement was included at the beginning of each motion trace. The prostate was shifted by 3 mm, 2 mm, and 2 mm in the posterior, inferior and right directions respectively. This interfraction displacement was selected based on the root-mean-square deviations of internal prostate displacements with respect to the bony anatomy measured by Bylund *et al* (2008). The selected prostate motion traces are shown in figure 3. The lymph nodes were assumed to be fixed to the vasculature and remained static (Shih *et al* 2005). In a practical treatment scenario on a standard linac, the position of the prostate would be monitored through on-board imaging of implanted fiducial markers, and the lymph nodes could be monitored by using the bony anatomy as a surrogate.

For both the dose-optimised and geometric-optimised MLC tracking treatment simulations, patients were set up to the bony anatomy and the prostate motion was managed using MLC tracking. Thus, each tracking strategy corrected for prostate motion that included both interfraction and intrafraction displacement. For the no tracking strategy, the patient was set up to the position of the prostate to replicate the dose that would be delivered during the standard of care. Using this patient setup, the prostate motion began at zero and instead displaced the lymph nodes by 3 mm, 2 mm, and 2 mm in the anterior, superior, and left directions respectively.

Fast dose error

To assess the performance of the leaf optimisation method to minimise dosimetric differences, the doses accumulated in the dose point clouds using the fast dose calculation were evaluated. The doses delivered during each treatment method with motion were accumulated in the dose point clouds (shown in figure 2) and



compared to the planned dose delivered using the planned MLC apertures without motion, accumulated in the same volume using the fast dose calculation described in detail by Mejnertsen *et al* (2021). The delivered and planned doses calculated in the prostate and lymph node volumes with the fast dose calculation were compared using a 3D γ comparison with a 2% relative dose/2 mm distance-to-agreement pass criterion, where the planned dose was considered the ground truth. Errors accumulated in the dose point clouds were considered to evaluate the capability of the MLC optimisation method to adapt the leaves to the given desired dose distribution, ignoring the error contribution that would result from the use of a simplified real-time dose accumulation algorithm.

Clinical dose error

While the multi-target dose-optimised MLC tracking method relies on a fast dose calculation to perform real-time adaptation, these dose point clouds are only an approximation. To evaluate the dosimetric error resulting from each of the treatment methods, the delivered doses were also calculated using a clinical treatment planning system (TPS) (Eclipse version 16.1, Varian Medical Systems, Palo Alto, California, USA).

Analysis of the clinical dose error was performed using a dose reconstruction method previously described by Poulsen *et al* (2012b). The DICOM plan files were first exported from the TPS. The DICOM plan for each patient was then modified using a computer code developed using MATLAB (MathWorks, Natick, Massachusetts, USA) where the prostate motion was encoded by dividing the plan into multiple sub-arcs, shifting the isocentre for each sub-arc corresponding to the displacement of the prostate divided into 1 mm bins.

For each treatment, two separate dose reconstructions were calculated in the TPS to reconstruct the clinical dose to the independently moving structures. One dose reconstruction encoded the prostate motion to evaluate the dose delivered to the moving structures which included the prostate, bladder, and rectum. The other dose reconstruction did not encode motion to evaluate the dose delivered to the static structures which included the lymph nodes and small bowel. Treatments using MLC tracking had the adapted MLC apertures encoded. Each DICOM file was then re-imported into the TPS and the doses were calculated with a grid size of $2.5 \times 2.5 \times 2.5 \text{ mm}^3$.

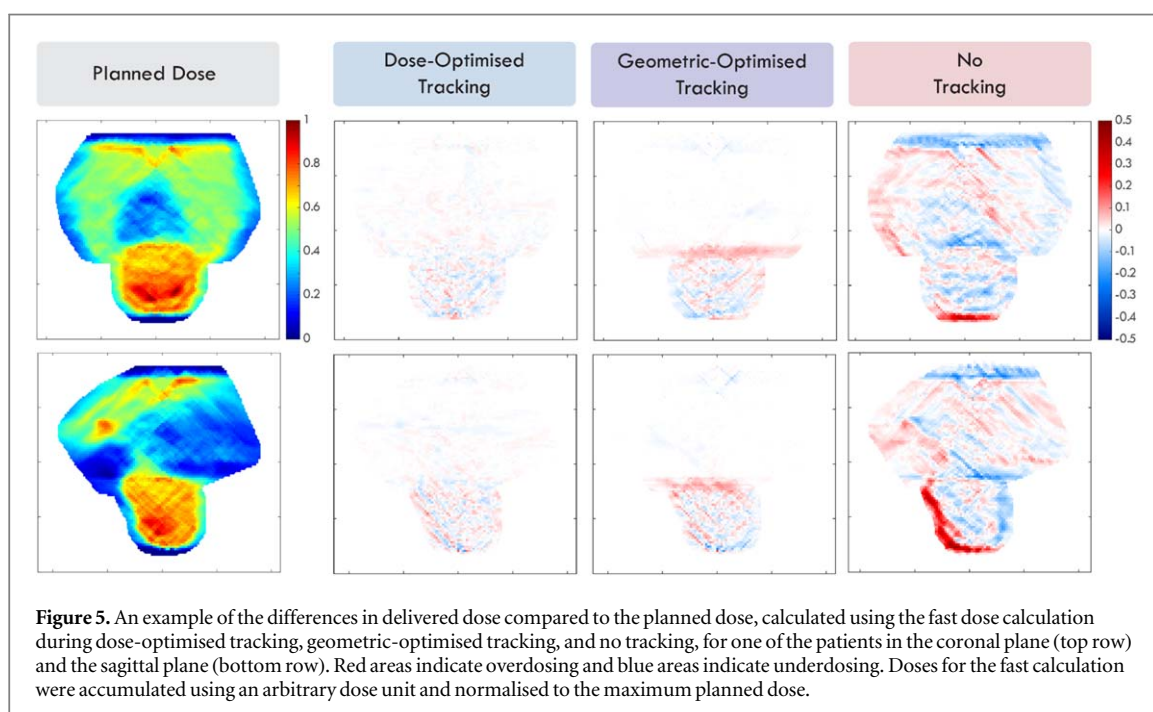
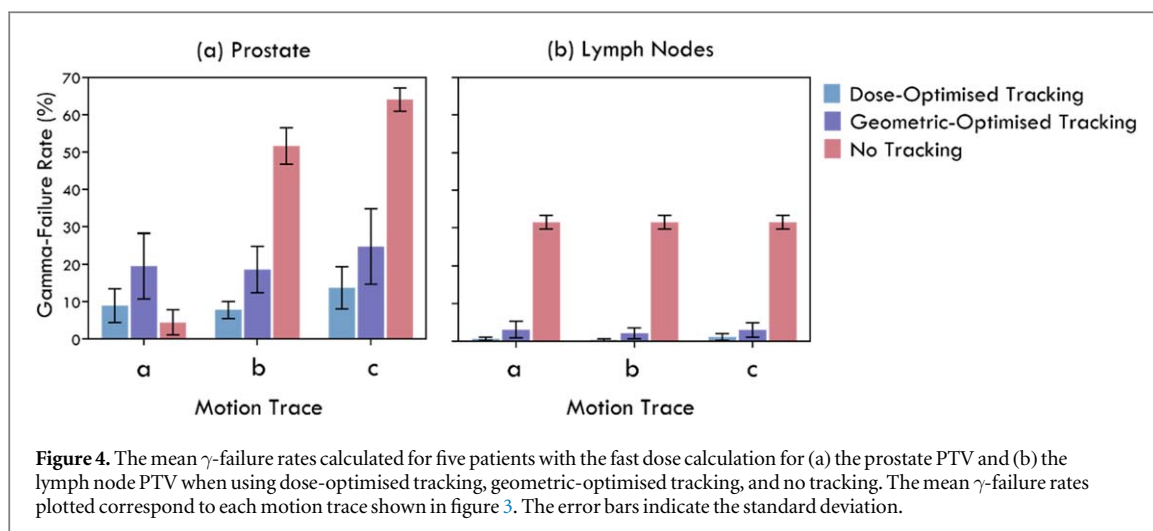
The doses calculated in the TPS were exported, and the delivered doses using each treatment method were compared to the planned dose volumes using a 3D γ comparison (Low and Dempsey 2003) with a 2%/2 mm criterion. The dose points contained within the contoured prostate and lymph nodes volumes were evaluated individually. Dose metrics for the prostate clinical target volume (CTV) and PTV, lymph node CTV and PTV, bladder, rectum and small bowel were also assessed compared to the planned values.

A Wilcoxon signed-rank test was performed to compare the γ -failure rates when dose-optimised multi-target MLC tracking was used, compared to when geometric-optimised multi-target MLC tracking, and no tracking were used.

Results

Fast dose error

The mean γ -failure rates for the comparison of the fast dose calculations across the five patients are plotted in figure 4. The overall mean γ -failure rate for the prostate and lymph nodes respectively were $10\% \pm 4.9\%$ and $0.7\% \pm 0.6\%$ for dose-optimised tracking, $30\% \pm 8.3\%$ and $2.7\% \pm 1.8\%$ for geometric-optimised tracking, and $39\% \pm 26\%$ and $32\% \pm 1.7\%$ when no tracking was used. Dose-optimised tracking had a statistically



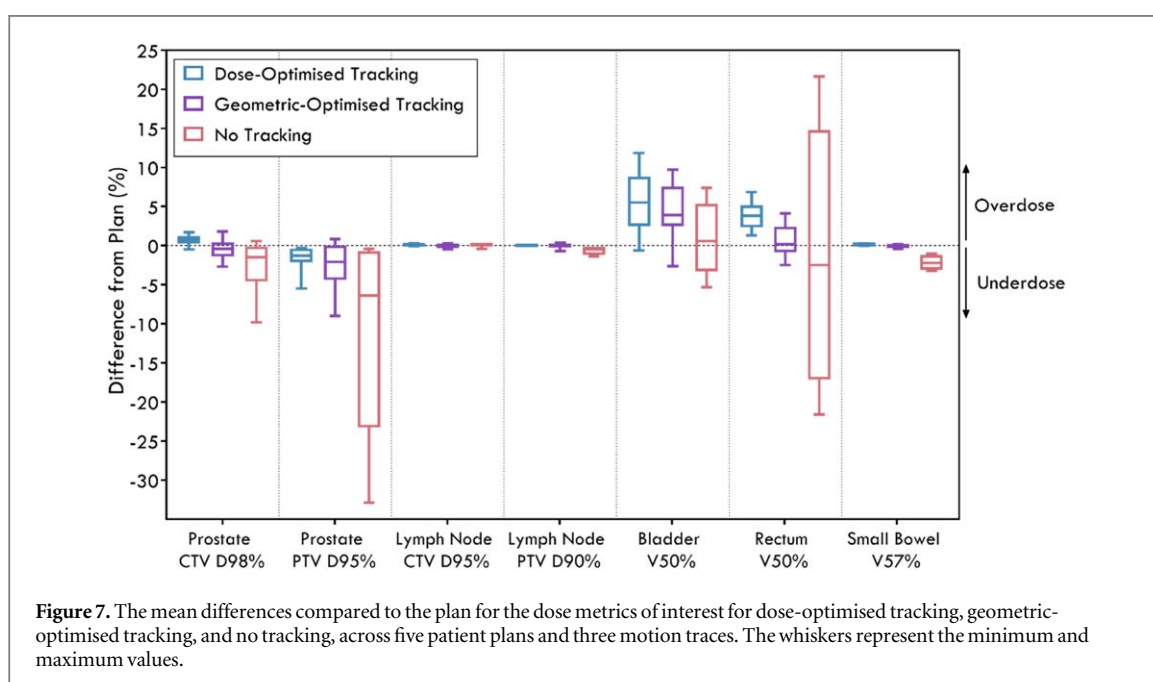
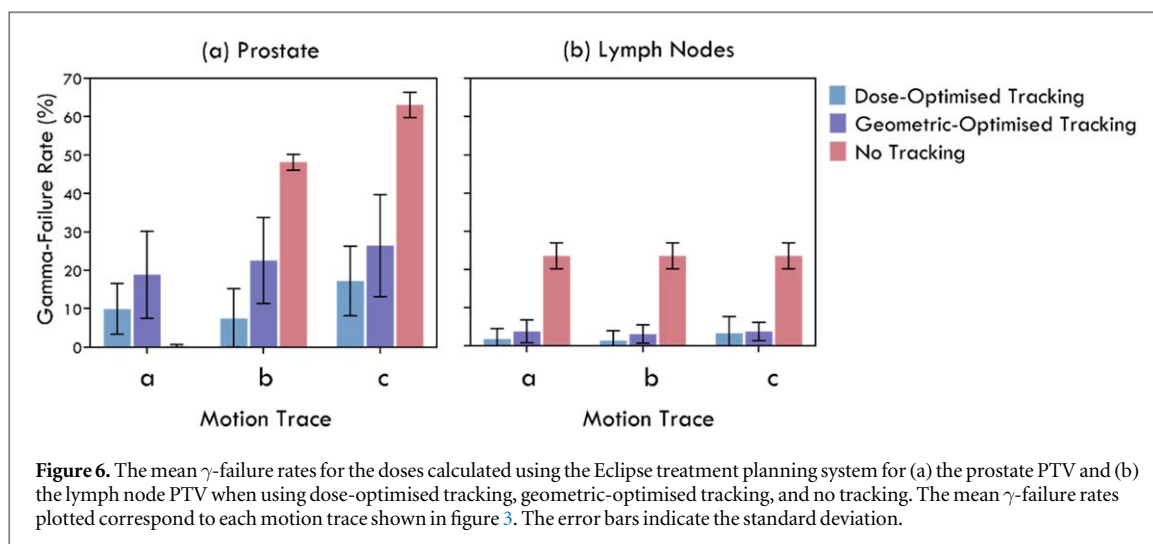
significantly lower mean γ -failure rate compared to both geometric-optimised tracking ($p < 0.001$ for the prostate and lymph nodes), and no tracking ($p = 0.008$ for the prostate, $p < 0.001$ lymph nodes). An example of the doses delivered to the dose point cloud for one of the patient plans using each treatment technique is shown in figure 5.

Clinical dose error

The mean γ -failure rates for the comparison of the clinical dose calculations across the five patients are plotted in figure 6. The overall mean γ -failure rate for the prostate and lymph nodes respectively were $12\% \pm 8.5\%$ and $1.8\% \pm 2.7\%$ for dose-optimised tracking, $23\% \pm 12\%$ and $3.6\% \pm 2.5\%$ for geometric-optimised tracking, and $37\% \pm 28\%$ and $24\% \pm 3.2\%$ when no tracking was used. Dose-optimised tracking had a statistically significantly lower mean γ -failure rate compared to both geometric-optimised tracking ($p < 0.001$ for the prostate, $p = 0.02$ for the lymph nodes), and no tracking ($p = 0.008$ for the prostate, $p < 0.001$ lymph nodes).

The difference between the planned dose and the reconstructed delivered doses for specific dose metrics of interest are plotted in figure 7.

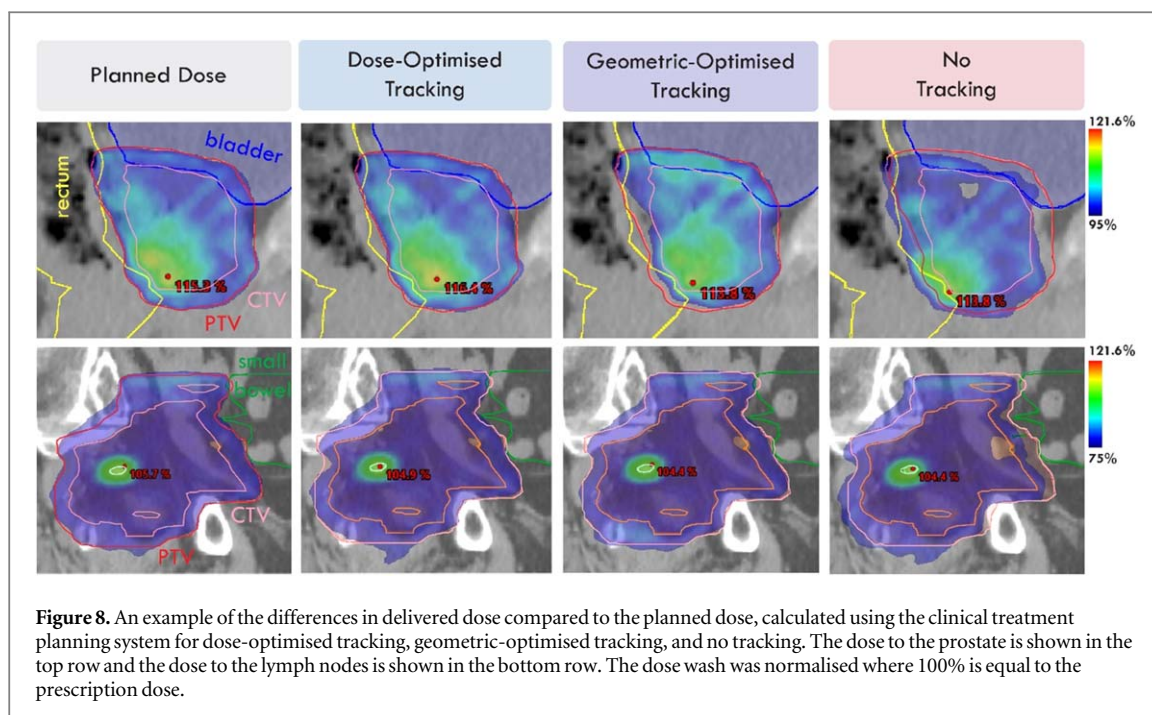
An example of the dose distributions calculated using the TPS is shown in figure 8. The same patient and motion trace that was plotted in figure 5 is also shown in figure 8 for the clinically calculated dose.



Discussion

In this study, a novel multi-target MLC tracking method was developed by optimising for the delivered 3D dose during treatment. Dose-based multi-target MLC tracking allowed for the prescribed dose to be delivered to targets that move independently from each other, paving the way for improved dose conformity for locally advanced cancer patients. This dose-optimised multi-target tracking method was evaluated through simulated treatments and compared to previously implemented methods including geometric-optimised MLC tracking, and the standard of care. The results demonstrated that an MLC tracking method that optimises the MLC leaves to correct for the real-time dose could be used to adapt treatment for multiple independent targets. This study also demonstrated that dose delivered using dose-optimised tracking would be closer to the planned dose distribution compared to both geometric-optimised tracking and no tracking.

Dose-optimised multi-target tracking had the lowest mean γ -failure rate when comparing the planned and delivered doses calculated in the TPS for both the prostate and lymph nodes. Dose-optimised multi-target tracking was also found to have the lowest γ -failure rate for all three motion traces with the exception of the prostate with the small prostate motion trace (figure 3(a)), where the no tracking method had the lowest γ -failure rate. This was due to the difference in patient set-up for the two methods. When MLC tracking was used the patient was set up to the lymph nodes so both interfraction and intrafraction prostate motion had to be corrected. When no tracking was used, the patient was set up to the prostate. The intrafraction prostate motion for this motion trace was small, so the dosimetric error in the prostate for the no tracking strategy remained low.



However, the no tracking strategy instead resulted in large dosimetric error to the lymph nodes. Due to the time delay between patient set-up and irradiation during real patient treatments, we may also expect the prostate to have deviated away from the zero position at the start of the first treatment arc, which would lead to larger dosimetric error to the prostate when motion is not tracked. Future real-time multi-target adaptation methods could be combined with online adaptive radiotherapy techniques to correct for the relative interfraction displacements between the primary target and lymph nodes (Thörnqvist *et al* 2013, Liu *et al* 2017).

Geometric-optimised multi-target tracking was able to reduce the overall mean dosimetric error compared to no tracking, but was found to have higher γ -failure rates compared to dose-optimised multi-target tracking for all three motion traces. As shown in figure 8, dose-optimised multi-target tracking did not result in overdosing in the region where the prostate and lymph nodes overlap, which can be seen when geometric-optimised multi-target tracking was used and was a notable limitation of the multi-target MLC tracking method that was observed previously (Hewson *et al* 2021a). There are still physical challenges with optimising the dose to multiple targets simultaneously by using the MLC leaves to correct for dose in the 2D BEV plane. Areas where the targets overlap in the BEV and are covered by the same leaf pair will be limited by what can best be achieved with a new MLC leaf position. While it is not guaranteed that all dose errors can be eliminated, dose-optimised tracking was able to deliver a dose that was more consistent with the plan compared to the previous methods for both targets.

Clinically relevant dose metrics from the reconstructed doses were also analysed (figure 7). Dose-optimised multi-target tracking had the smallest deviation from the plan for the prostate CTV $D_{98\%}$ and prostate PTV $D_{95\%}$, and the differences from the plan for the lymph node CTV $D_{95\%}$ and PTV $D_{90\%}$ were small for all three treatment strategies. One of the aims of developing a dose-optimised multi-target tracking strategy was to reduce the overdosing to the organs at risk (OARs). However, these improvements were not seen, with higher doses to the bladder $V_{50\%}$ and rectum $V_{50\%}$ when using dose-optimised multi-target tracking compared to geometric-optimised multi-target tracking. This was likely a result of the dose-optimisation algorithm only considering the dose points that exist within the PTVs, ignoring dose errors that occur outside of these regions, including the OARs. As the planned dose distribution to the OARs is determined by their proximities to the targets in the planning CT, delivering a dose that is consistent with what was planned to a target that has now undergone relative motion to the OAR will result in a dose to the OAR that is not consistent with what was planned. Instead, future improvements to the dose optimisation algorithm should include the OARs in the dose point cloud and avoid overdosing to the OARs by considering the clinical dose-volume constraints, optimising the adapted leaf positions to ensure that while target dose coverage is achieved, the planning constraints for the OARs are not violated during treatment. This would require a more advanced version of the dose-optimisation algorithm where future gantry angles are also considered to determine the optimal MLC apertures that would allow for OAR avoidance given the updated anatomy. Additionally, the current method assumes that the targets undergo rigid translation, so a more complex motion model that includes organ deformation could be used to capture the motion of the OARs more accurately in the vicinity of the prostate target. However, without intrafraction

volumetric images, the dose cannot be optimised to the actual anatomy and assumptions based on the anatomy in the planning CT will have to be made.

Similar to the doses analysed in the clinical TPS, the γ -failure rates for the fast dose calculations were found to be lowest for dose-optimised tracking overall, and the relative performance of each tracking method in figure 6 showed similar trends to the results in figure 4. The overdosing to the targets near the overlapping region seen in figure 5 for geometric-optimised tracking was also reflected in figure 8 where a higher dose can be seen near the base of the prostate when using geometric-optimised tracking, as well as some loss in coverage to the posterior part of the prostate PTV. However, the dosimetric errors observed using the clinically calculated dose were slightly higher compared to the fast dose calculations. This suggests that there may be some contribution to the error resulting from using a fast dose calculation to guide the adapted MLC leaf optimisation. It should also be noted that some differences in the observed γ -failure rates may also be a result of the different voxel resolutions between the two dose calculation methods (a staggered grid with a 2 mm spacing for the dose point cloud and a $2.5 \times 2.5 \times 2.5 \text{ mm}^3$ dose grid size for the clinical dose calculation).

Previous methods have investigated adapting treatment decisions in response to the dose accumulated during the treatment. Wisotzky *et al* (2016) investigated MLC aperture optimisation based on the accumulated errors throughout the treatment, however, this study was limited to correcting for 2D under- and over-exposure for conformal and intensity-modulated radiotherapy (IMRT). Kontaxis *et al* (2015a, 2015b) similarly developed an algorithm to adapt step-and-shoot IMRT treatment to anatomical changes but optimised the fluence map for each MLC segment based on a 3D dose calculation. While Kontaxis *et al* applied a similar principle to that used in the current study, their method did not occur on a sub-second timescale and would not be suitable for VMAT treatment. Muurholm *et al* (2021) achieved improved dosimetric accuracy through couch corrections guided by dose accumulated to the treatment target, but were limited by rigid translations of a single target to correct for dose error, and interruptions to treatment. Kamerling *et al* (2016) demonstrated real-time dose reconstruction that calculated the doses delivered to a moving target volume with MLC tracking for lung stereotactic body radiation therapy, however this dosimetric information was not fed back into the MLC tracking algorithm to guide treatment adaptation.

This study reported the first analysis of the performance of dose-optimised MLC tracking using clinical dose calculations in a TPS. While dosimetric errors did slightly increase for the clinical dose analysis, dose-optimised tracking was still found to have the lowest γ -failure rates, suggesting that although the fast dose calculation only models zeroth-order dose deposition, it was still sufficient to perform dose-optimised tracking and improve treatment over the other methods. However, the dosimetric accuracy of this algorithm could be further improved by using a more advanced dose calculation algorithm. Ravkilde *et al* (2014) have developed a fast real-time dose calculation method based on the use of a simplified version of a pencil beam convolution algorithm (Storchi and Woudstra 1995, 1996, Storchi *et al* 1999) that was implemented in the Eclipse TPS. Real-time dose calculations performed using this method were shown to be accurate with mean differences between the real-time dose calculation and the measured doses of within $-1.5\% \pm 3.9\%$ for the cumulative dose (Ravkilde *et al* 2018). Improved dose calculation algorithms with tissue density modelling may be necessary when applying dose-optimised adaptation methods for anatomical sites with higher heterogeneity such as the lung. Future fast dose calculation algorithms could also improve dose-optimised MLC tracking by accounting for additional factors such as varying field sizes and the depth of dose deposition. Implementing more realistic dose-calculations to guide MLC leaf optimisation may however require a compromise between dosimetric accuracy and computational time.

Improvements to the MLC leaf optimisation method could also reduce the dosimetric errors observed in this study. Currently the dose-optimisation algorithm assigns equal weight to both overdosing and underdosing to the entire dose point cloud. Future developments to this algorithm could look to include additional dose points that discriminate between those belonging to the targets and the OARs and translate these dose points according to how the OARs move as well as the targets. This would allow for the algorithm to further penalise overdosing to the OARs and underdosing to the targets. This could potentially reduce the dosimetric errors to the bladder and rectum that was observed in figure 7.

One drawback to the dose-optimised MLC tracking method is that performance was found to be dependent on the planned collimator angles. Originally the locally advanced prostate cancer treatment plans were generated using angles of 10° , 350° and 0° , but dose corrections performed in the BEV were not as effective due to the resulting geometry where the direction of leaf motion was in the same plane of the gantry rotation. This limitation was managed by replanning these patients with collimator angles of 45° and 315° as these angles were found to be favourable to reduce the dosimetric error. However, these collimator angles are not used in standard treatment and resulted in lower quality plans for target coverage and OAR sparing, so a decision would have to be made whether the benefit gained by performing dose-optimised tracking outweighs a potential reduction in plan quality. Dose-optimised tracking should be further improved to allow for adequate dose error corrections independent of the planned collimator angle. Despite the limitations of dose-optimised multi-target tracking, of

which there are pathways to overcome, the results with the dose-optimisation method that has been implemented still demonstrated the ability to track multiple targets with lower dose error compared to previous methods.

Conclusion

This study developed a novel multi-target MLC tracking method that optimised the MLC leaves based on minimising the difference between the delivered and planned doses to complex dynamic anatomy in real-time. The results demonstrated that dose-optimised multi-target MLC tracking was able to reduce dosimetric errors to two independently moving targets. There is a desire for real-time adaptive radiotherapy to be transitioned into standard clinical practice and dose-optimised multi-target tracking provides one pathway toward this goal, offering a unique solution that is accessible on current treatment machines with the potential to further improve patient outcomes.

Acknowledgments

The authors acknowledge funding from the Cancer Council NSW (1165097). The authors would also like to thank Dr Helen Ball and Dr Hilary Byrne for reviewing the manuscript.

ORCID iDs

Emily A Hewson  <https://orcid.org/0000-0001-7353-2663>

Doan Trang Nguyen  <https://orcid.org/0000-0003-1581-0359>

Lars Mejnertsen  <https://orcid.org/0000-0003-0710-0744>

References

- Booth J *et al* 2021 MLC tracking for lung SABR is feasible, efficient and delivers high-precision target dose and lower normal tissue dose *Radiother. Oncol.* **155** 131–7
- Bylund K C, Bayouth J E, Smith M C, Hass A C, Bhatia S K and Buatti J M 2008 Analysis of interfraction prostate motion using megavoltage cone beam computed tomography *Int. J. Radiat. Oncol. * Biol. * Phys.* **72** 949–56
- Dale R 1996 Dose-rate effects in targeted radiotherapy *Phys. Med. Biol.* **41** 1871–84
- Falk M *et al* 2010 Real-time dynamic MLC tracking for inversely optimized arc radiotherapy *Radiother. Oncol.* **94** 218–23
- Grimm J, Marks L B, Jackson A, Kavanagh B D, Xue J and Yorke E 2021 High dose per fraction, hypofractionated treatment effects in the clinic (HyTEC): an overview *Int. J. Radiat. Oncol. * Biol. * Phys.* **110** 1–10
- Hewson E A *et al* 2021a Adapting to the motion of multiple independent targets using multileaf collimator tracking for locally advanced prostate cancer: proof of principle simulation study *Med. Phys.* **48** 114–24
- Hewson E A *et al* 2021b First experimental evaluation of multi-target multileaf collimator tracking during volumetric modulated arc therapy for locally advanced prostate cancer *Radiother. Oncol.* **160** 212–20
- Hwang A, Chen J, Nguyen T, Gottschalk A, Roach M III and Pouliot J 2012 Irradiation of the prostate and pelvic lymph nodes with an adaptive algorithm *Med. Phys.* **39** 1119–24
- Kamerling C P, Fast M F, Ziegenhein P, Menten M J, Nill S and Oelfke U 2016 Real-time 4D dose reconstruction for tracked dynamic MLC deliveries for lung SBRT *Med. Phys.* **43** 6072–81
- Keall P J *et al* 2018a Electromagnetic-guided MLC tracking radiation therapy for prostate cancer patients: prospective clinical trial results *Int. J. Radiat. Oncol. * Biol. * Phys.* **101** 387–95
- Keall P J *et al* 2018b The first clinical implementation of real-time image-guided adaptive radiotherapy using a standard linear accelerator *Radiother. Oncol.* **127** 6–11
- Keall P J *et al* 2021 AAPM Task group 264: the safe clinical implementation of MLC tracking in radiotherapy *Med. Phys.* **48** e44–64
- Kershaw L, van Zadelhoff L, Heemsbergen W, Pos F and van Herk M 2018 Image guided radiation therapy strategies for pelvic lymph node irradiation in high-risk prostate cancer: motion and margins *Int. J. Radiat. Oncol. * Biol. * Phys.* **100** 68–77
- Kilby W, Dooley J, Kuduvalli G, Sayeh S and Maurer C Jr 2010 The cyberknife[®] robotic radiosurgery system in 2010 *Technol. Cancer Res. Treat.* **9** 433–52
- Kontaxis C, Bol G H, Lagendijk J J W and Raaymakers B W 2015a Towards adaptive IMRT sequencing for the MR-linac *Phys. Med. Biol.* **60** 2493–509
- Kontaxis C, Bol G H, Lagendijk J J W and Raaymakers B W 2015b A new methodology for inter- and intrafraction plan adaptation for the MR-linac *Phys. Med. Biol.* **60** 7485–97
- Langen K M *et al* 2008 Observations on real-time prostate gland motion using electromagnetic tracking *Int. J. Radiat. Oncol. * Biol. * Phys.* **71** 1084–90
- Liu F, Tai A, Ahunbay E, Gore E, Johnstone C and Li X A 2017 Management of independent motion between multiple targets in lung cancer radiation therapy *Pract. Radiat. Oncol.* **7** 26–34
- Liu P Z *et al* 2020 First experimental investigation of simultaneously tracking two independently moving targets on an MRI-linac using real-time MRI and MLC tracking *Med. Phys.* **47** 6440–9
- Low D A and Dempsey J F 2003 Evaluation of the gamma dose distribution comparison method *Med. Phys.* **30** 2455–64
- Mejnertsen L, Hewson E, Nguyen D T, Booth J and Keall P 2021 Dose-based optimisation for multi-leaf collimator tracking during radiation therapy *Phys. Med. Biol.* **66** 065027

- Moore D, Ruan D and Sawant A 2016 Fast leaf-fitting with generalized underdose/overdose constraints for real-time MLC tracking *Med. Phys.* **43** 465–74
- Muurholm C G et al 2021 Real-time dose-guidance in radiotherapy: proof of principle *Radiother. Oncol.* **164** 175–82
- Olsson C E, Jackson A, Deasy J O and Thor M 2018 A systematic post-QUANTEC review of tolerance doses for late toxicity after prostate cancer radiation therapy *Int. J. Radiat. Oncol. *Biol. *Phys.* **102** 1514–32
- Pantarotto J R, Piet A H, Vincent A, de Koste J R V S and Senan S 2009 Motion analysis of 100 mediastinal lymph nodes: potential pitfalls in treatment planning and adaptive strategies *Int. J. Radiat. Oncol. *Biol. *Phys.* **74** 1092–9
- Poulsen P R, Fledelius W, Cho B and Keall P 2012a Image-based dynamic multileaf collimator tracking of moving targets during intensity-modulated arc therapy *Int. J. Radiat. Oncol. *Biol. *Phys.* **83** e265–71
- Poulsen P R, Schmidt M L, Keall P, Worm E S, Fledelius W and Hoffmann L 2012b A method of dose reconstruction for moving targets compatible with dynamic treatments *Med. Phys.* **39** 6237–46
- Ravkilde T, Keall P J, Grau C, Høyer M and Poulsen P R 2014 Fast motion-including dose error reconstruction for VMAT with and without MLC tracking *Phys. Med. Biol.* **59** 7279–96
- Ravkilde T, Skouboe S, Hansen R, Worm E and Poulsen P R 2018 First online real-time evaluation of motion-induced 4D dose errors during radiotherapy delivery *Med. Phys.* **45** 3893–903
- Ruan D and Keall P 2011 Dynamic multileaf collimator control for motion adaptive radiotherapy: an optimization approach 2011 *IEEE Power Engineering and Automation Conf.* (Piscataway, NJ: IEEE) (<https://doi.org/10.1109/PEAM.2011.6135024>)
- Sawant A et al 2008 Management of three-dimensional intrafraction motion through real-time DMLC tracking *Med. Phys.* **35** 2050–61
- Schmidt M L et al 2016 Cardiac and respiration induced motion of mediastinal lymph node targets in lung cancer patients throughout the radiotherapy treatment course *Radiother. Oncol.* **121** 52–8
- Schnarr E et al 2018 Feasibility of real-time motion management with helical tomotherapy *Med. Phys.* **45** 1329–37
- Shih H A, Harisinghani M, Zietman A L, Wolfgang J A, Saksena M and Weissleder R 2005 Mapping of nodal disease in locally advanced prostate cancer: rethinking the clinical target volume for pelvic nodal irradiation based on vascular rather than bony anatomy *Int. J. Radiat. Oncol. *Biol. *Phys.* **63** 1262–9
- Storchi P, Van Battum L and Woudstra E 1999 Calculation of a pencil beam kernel from measured photon beam data *Phys. Med. Biol.* **44** 2917–28
- Storchi P and Woudstra E 1995 Calculation models for determining the absorbed dose in water phantoms in off-axis planes of rectangular fields of open and wedged photon beams *Phys. Med. Biol.* **40** 511–27
- Storchi P and Woudstra E 1996 Calculation of the absorbed dose distribution due to irregularly shaped photon beams using pencil beam kernels derived from basic beam data *Phys. Med. Biol.* **41** 637–56
- Thörnqvist S et al 2013 Adaptive radiotherapy in locally advanced prostate cancer using a statistical deformable motion model *Acta Oncol.* **52** 1423–9
- van Elmpt W, Öllers M, Lambin P and De Ruyscher D 2012 Should patient setup in lung cancer be based on the primary tumor? an analysis of tumor coverage and normal tissue dose using repeated positron emission tomography/computed tomography imaging *Int. J. Radiat. Oncol. *Biol. *Phys.* **82** 379–85
- Weiss E, Robertson S P, Mukhopadhyay N and Hugo G D 2012 Tumor, lymph node, and lymph node-to-tumor displacements over a radiotherapy series: analysis of interfraction and intrafraction variations using active breathing control (ABC) in lung cancer *Int. J. Radiat. Oncol. *Biol. *Phys.* **82** e639–45
- Wijesooriya K, Bartee C, Siebers J V, Vedam S S and Keall P J 2005 Determination of maximum leaf velocity and acceleration of a dynamic multileaf collimator: implications for 4D radiotherapy *Med. Phys.* **32** 932–41
- Wisotzky E, O'Brien R and Keall P J 2016 A novel leaf sequencing optimization algorithm which considers previous underdose and overdose events for MLC tracking radiotherapy *Med. Phys.* **43** 132–6